RSC Applied Polymers

ROYAL SOCIETY OF CHEMISTRY

PAPER

View Article Online
View Journal | View Issue

Check for updates

Cite this: *RSC Appl. Polym.*, 2025, **3**, 209

# Nafion membranes for power generation from physiologic ion gradients†

Carolina Pierucci, [a,e] Lorenzo Paleari, [b] James Baker, [a,c,e] Christian C. M. Sproncken, [a,e] Matilde Folkesson, [a] Justus Paul Wesseler, [a] Andela Vracar, [a] Andrea Dodero, [a,e] Francesca Nanni, [b] José Augusto Berrocal, [a,f] Michael Mayer *[a,e] and Alessandro Ianiro *[a,d,e]

Received 24th September 2024,
Accepted 18th November 2024

DOI: 10.1039/d4lp00294f

rsc.li/rscapplpolym

Creatures such as torpedo rays and electric eels showcase the exceptional ability to convert ionic gradients inside their bodies into powerful electrical discharges. In the future, artificial power units capable of reproducing this intriguing biological phenomenon may be able to power active devices, such as pacemakers and prosthetics, directly from ion gradients present in the human body. The present work evaluates the use of proton-selective Nafion membranes to generate electric power from the pH gradient present in the human stomach. First, we characterize two different commercial Nafion membranes by focusing on their ion exchange performance. In particular, we quantify the perm-selectivity of these membranes for various hydrated ions relative to that of the hydronium ion. Our results indicate that the transport of ions in wet Nafion proceeds through water-filled nanochannels, and that proton selectivity can be explained simply by the much larger mobility of protons in water with respect to other ions. Subsequently, we demonstrate a Nafion-based artificial electric organ capable of generating electric power from gastric juices. This power unit is built according to the reverse electrodialysis (RED) scheme, with each cell stack in series capable of generating 134 mV of potential difference and 188 mW $m^{-2}$ of power density.

Open Access Article. Published on 19 2024. Downloaded on 26-06-2025 08:06:16.
This article is licensed under a Creative Commons Attribution-NonCommercial 3.0 Unported Licence.

## Introduction

The World Health Organization has reported that 35–40 million people worldwide, (approximately 0.5% of the global population) need prosthetic devices.[1] Robotic prosthetics are consequently gaining significance as they enable the partial restoration of lost physical functionalities. These active devices, however, present a major limitation as they require periodic recharging and cannot operate continuously without external energy sources. A compelling strategy to circumvent this limitation is developing devices that can harvest energy directly from the human body and use it to power these active prosthetics.[2–4] This approach provides a continuous and sustainable energy source by directly utilizing metabolic energy, thus eliminating the need for periodic recharging and external power sources. This approach is especially relevant in the context of biomedical, implantable, and wearable devices, whose functioning typically relies on the use of batteries, which in some cases (*e.g.*, in pacemakers) need to be surgically replaced through invasive procedures.

Electric fish possess the remarkable ability to produce powerful electrical discharges through the manipulation of ion fluxes across ion-selective membranes within their bodies.[5] Mimicking the bioelectric phenomena taking place in the electric organ of electric fish is a promising route to develop artificial electric organs.[6,7] The mechanism underlying the production of electric power in electric fish resembles, under many aspects, the reverse electrodialysis (RED) process. In RED, an alternating stack of cation exchange membranes (CEM) and anion exchange membranes (AEM) separates alternating ion-poor and ion-rich solutions, as shown in Fig. 1A. This arrangement favors the displacement of positive charges toward one side and negative charges toward the opposite side of the system, leading to a net flux of charges and additive transmembrane potentials. A pair of electrodes is used to harness this ionic current.[8–10]

[a]*Adolphe Merkle Institute, University of Fribourg, Chemin des Verdiers 4, CH-1700 Fribourg, Switzerland. E-mail: alessandro.ianiro@kuleuven.be, alessandro.ianiro@unifr.ch, michael.mayer@unifr.ch*
[b]*Dep. Enterprise Engineering, University of Rome Tor Vergata, Via del Politecnico 1, 00133 Rome, Italy*
[c]*Dep. Electrical Engineering, Saint Louis University, 1 N Grand Blvd, Saint Louis, Missouri, USA*
[d]*Dep. of Chemistry, Catholic University of Leuven, Celestijnenlaan 200F, 3001 Leuven, Belgium*
[e]*National Center for Competence in Research (NCCR) Bio-inspired Materials, University of Fribourg, Chemin des Verdiers 4, CH-1700 Fribourg, Switzerland*
[f]*Institute of Chemical Research of Catalonia (ICIQ), Barcelona Institute of Science and Technology (BIST), Av. Països Catalans, 16, Tarragona, E-43007, Spain*
†Electronic supplementary information (ESI) available: Supplementary Fig. S1–S13. See DOI: https://doi.org/10.1039/d4lp00294f

© 2025 The Author(s). Published by the Royal Society of Chemistry

Open Access Article. Published on 19 2024. Downloaded on 26-06-2025 08:06:16.
This article is licensed under a Creative Commons Attribution-NonCommercial 3.0 Unported Licence.

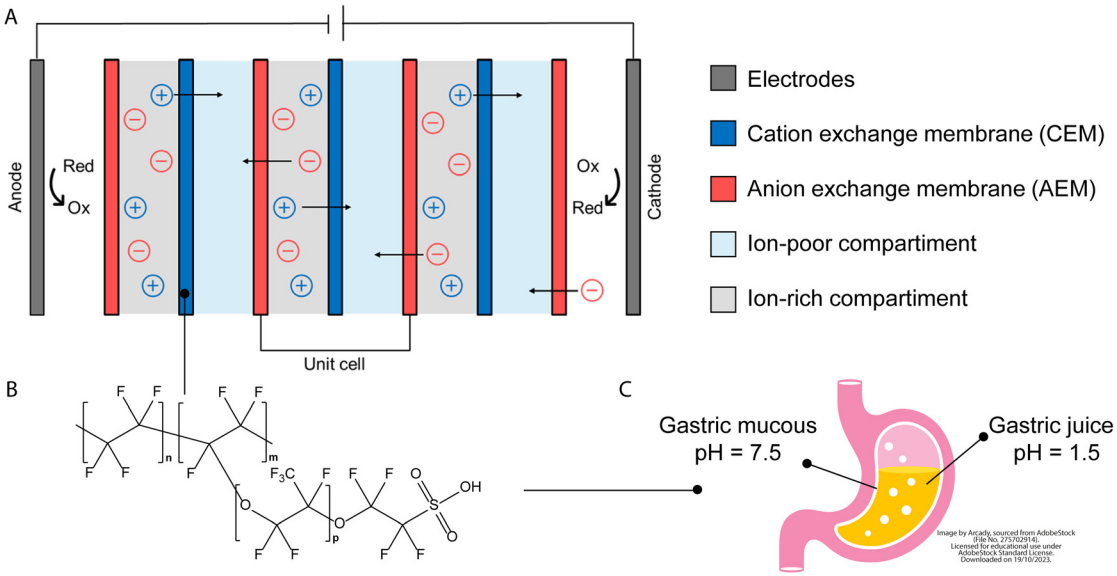


**Fig. 1** (A) Mechanism of power generation in reverse electrodialysis. Due to the ionic gradient between the ion-poor and ion-rich compartments, a potential is produced across the alternating ion-selective membranes (CEM and AEM) that is additive when the various unit cells are stacked in series. (B) Chemical structure of Nafion. (C) pH gradient inside the human stomach. Gastric juices have a pH close to 1.5, while gastric mucous has a pH of around 7.5 to neutralize the acidic pH of the juices and protect the walls of the organ. The stomach can be a possible candidate for implanting the artificial electric organ due to its metabolically maintained ionic gradient.

Membranes play a central role in RED as the energy conversion efficiency is linked to their ion- selectivity and permeability. Furthermore, the composition of the ion-rich and ion-poor solutions is critical and must be optimized to achieve the best tradeoff between electrical resistance (which limits current) and gradient of ions (which limits potential).[11–14]

Mayer's group at Adolphe Merkle Institute (Fribourg, Switzerland) has pioneered the realization of soft, hydrogel-based bioinspired power units[6,7] and has developed RED systems capable of generating electric power from exhaled carbon dioxide ($CO_2$), which is a metabolic byproduct.[15] The applicability of these devices in the human body is limited because hydrogel power sources undergo degradation under physiological conditions and are difficult to recharge *in vivo*, while capturing $CO_2$ from human breath requires the use of potentially harmful carbon-capturing agents such as ethanolamine.[15]

In this work, we evaluate the use of Nafion (Fig. 1B) as a proton exchange membrane (PEM) for the construction of artificial electric organs that convert the pH gradient of gastric solutions (Fig. 1C) into electric power. The pH gradient between gastric juices (pH ≈ 1.5)[16] and gastric mucous (pH ≈ 7.5)[17] is ideal for the development of an implantable electric organ because it is rather steep (*i.e.*, six orders of magnitude in proton concentration), is continuously maintained by the metabolism, and is readily accessible.

Nafion,[18] a sulfonated fluoropolymer, displays good proton exchange performance, and is widely applied in fuel cells for application in gas and liquid phases. The proton exchange properties of Nafion derive from its structure, which comprises a fluorinated backbone conferring hydrophobic properties, mechanical support and chemical stability, and sulfonated groups enabling selective cation exchange (Fig. 1B).[19–22] Moreover, Nafion exhibits exceptional thermal and chemical stability, withstanding temperatures well beyond the internal human body temperature (up to 150 °C or higher)[23] and remaining stable even in highly acidic conditions (10 M nitric acid for hours[24] and 1 M HCl for months).[18] These properties make it a compelling candidate for applications involving prolonged contact with the gastric juice-mimicking solution. One potential issue that could affect the performance of Nafion membranes is fouling. It is known that these membranes, when used in microbial fuel cell applications, can be passivated by a thin layer of bacteria after approximately six months of use.[25]

Despite recent environmental and biosafety guidelines discouraging the use of fluoropolymers in favor of more biodegradable and environmentally friendly alternatives,[26–29] however, we focused on Nafion because it still represents the golden standard in PEM. The success of Nafion, especially in fuel cell applications, is justified by its excellent proton conductivity.[30]

First, we discuss the use of gastric juices and gastric mucous as ion-rich and ion-poor solutions for power generation in a Nafion-based RED setup. Subsequently, we provide a detailed characterization of the ion exchange performance of two different commercial Nafion membranes: Xion PEM-Nafion-1100 (5 μm thick), and Nafion® 115 perfluorinated membrane (127 μm thick). In particular, we (i) quantify the perm-selectivity of these membranes for various hydrated cations relative to that of the hydronium ion, (ii) correlate these results to the structure of the membranes and the hydrodynamic properties of the cations, and (iii) use the measured


© 2025 The Author(s). Published by the Royal Society of Chemistry

Open Access Article. Published on 19 2024. Downloaded on 26-06-2025 08:06:16.
This article is licensed under a Creative Commons Attribution-NonCommercial 3.0 Unported Licence.

perm-selectivities to explain the potential generated by gastric juices and gastric mucous mimics across Nafion membranes.

Finally, we present an artificial electric organ that replaces gastric mucus with drinkable water as a low-salinity compartment to achieve a substantial increase in power output. Such a device represents the benchtop prototype of an implantable electric organ that can be recharged by simply drinking water to aliment low-power electronics and small prosthetics.

## Results and discussion

### Power generation from mimic solutions of gastric juices and gastric mucous

To estimate how much electric power we can harvest from gastric juices and gastric mucous across Nafion membranes, we designed a single-cell device (Fig. 2A) comprising two chambers separated by the Nafion membrane of interest. We filled one chamber with a solution simulating gastric juices (GJ) and the other with a solution mimicking gastric mucous (GM). The gastric juices mimic contained $Na^+$ (0.149 M), $H_3O^+$ (0.047 M, pH = 1.3), $OH^-$ ($2.1 \times 10^{-13}$ M), and $Cl^-$ (0.196 M), while the gastric mucus solution contained $Na^+$ (0.124 M), $K^+$ (0.005 M), $Cl^-$ (0.127 M), $H_3O^+$ ($2.2 \times 10^{-8}$ M, pH = 7.6), $OH^-$ ($4.5 \times 10^{-7}$ M), and $HCO_3^-$ (0.002 M). The overall ionic strengths of these solutions are similar ($I$ = 0.196 M for GJ and $I$ = 0.129 M for GM), but they are characterized by a large difference in the concentration of hydronium ions.

We placed an Ag/AgCl electrode in each chamber to measure both the open circuit voltage of the device ($V_{OC}$) and the internal resistance of the cell $r$ (see Methods for details). These two quantities enable to estimate the maximum achievable power density:[31]

$$PD_{max} = \frac{V_{OC}^2}{4rA}, \quad (1)$$

where $A$ is the area of the membrane.

For a single-membrane device using Ag/AgCl electrodes, the value of $V_{OC}$ is the sum of a contribution from the membrane ($V_M$) and a contribution from the electrodes ($V_{El}$):

$$V_{OC} = V_M + V_{El} \quad (2)$$

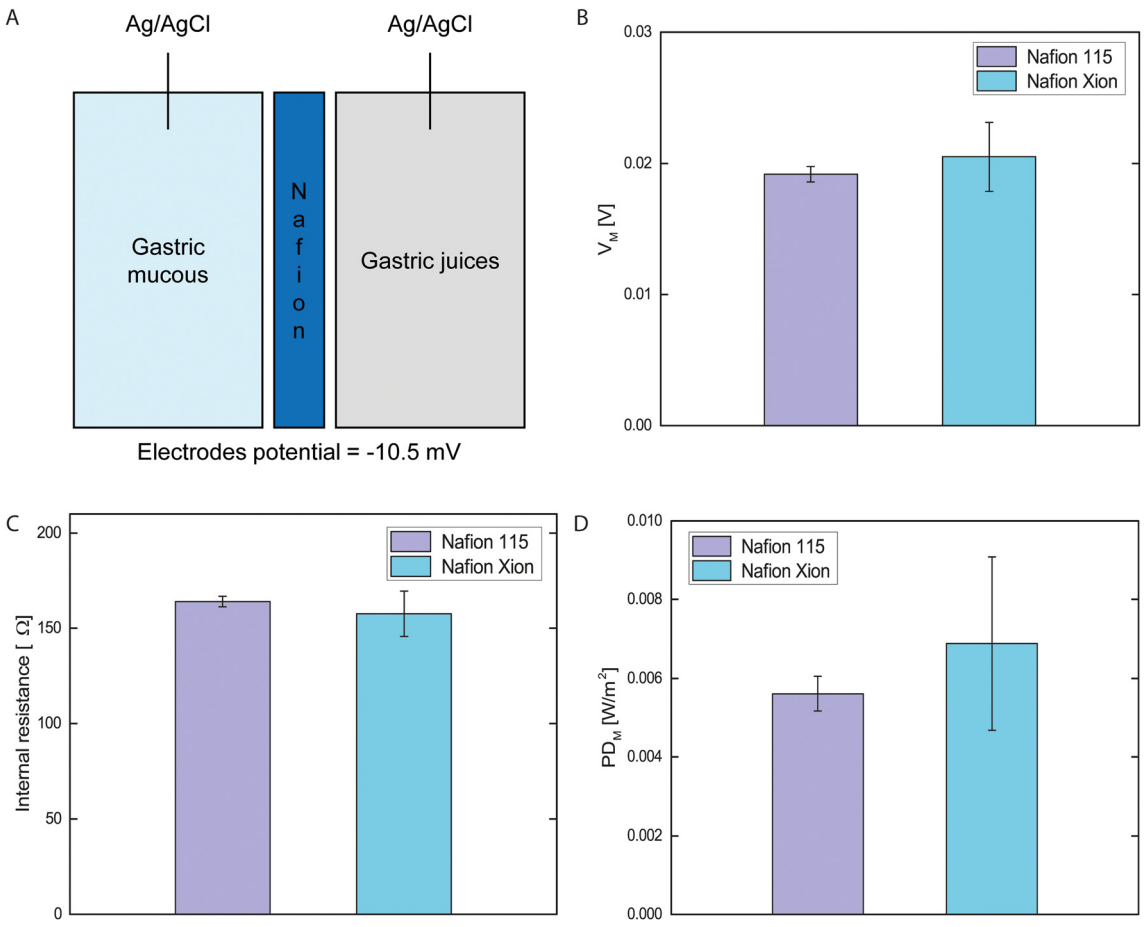


Fig. 2 (A) Schematic representation of the cell used to measure the voltage across Nafion membranes using gastric juices as ion-rich solution and gastric mucous as ion-poor solution. (B–D) Comparison of the (B) membrane potentials, (C) internal resistance, and (D) power density (from eqn (4)) obtained with Nafion® 115 and Xion with the setup reported in A.

© 2025 The Author(s). Published by the Royal Society of Chemistry

Open Access Article. Published on 19 2024. Downloaded on 26-06-2025 08:06:16.
This article is licensed under a Creative Commons Attribution-NonCommercial 3.0 Unported Licence.

In the case of Ag/AgCl electrodes, the contribution from the electrodes originates from the different chloride concentrations in the gastric mucus and gastric juices solutions and can be estimated using the Nernst equation:[32]

$$V_{El} = -\frac{RT}{nF}\log\frac{a_{GJ}^{Cl^-}}{a_{GM}^{Cl^-}} \approx 10\,\text{mV}, \quad (3)$$

where $R$ is the gas constant, $T$ is the temperature expressed in [K], $F$ is the Faraday constant, $n$ is the number of electrons transferred in the reaction, and $a_{GM}^{Cl^-}$ and $a_{GJ}^{Cl^-}$ are the activities of chloride ions in the solution mimicking GM and GJ, respectively.

The power density calculated using eqn (1) incorporates a contribution from $V_{El}$. The maximum power density attainable by a single Nafion membrane without the contribution of the electrodes is:

$$PD_M = \frac{V_M^2}{4rA}. \quad (4)$$

We tested two commercial Nafion membranes, namely Xion PEM-Nafion-1100 (5 μm thick), and Nafion® 115 (127 μm thick). The values of $V_M$, $r$ and $PD_M$ obtained with these two membranes are plotted in Fig. 2B–D. For both membranes, the measured $V_{OC}$ values were approximately, in the order of 30 mV. Subtracting the calculated value of $V_{El}$, we estimated a transmembrane potential $V_M \approx 20$ mV, which is surprisingly low considering that the concentration gradient of hydronium ions across the membranes spans six orders of magnitudes. Such low $V_M$ values limit the maximum attainable power density (Fig. 2D) and suggest that Nafion is not very selective for hydronium ions over the other hydrated cations present in solution ($K^+$ and $Na^+$). We verify this hypothesis in the next section, where we present an extensive characterization of the ion exchange performance of Nafion in aqueous environment. Nonetheless, we conclude that Nafion membranes, despite being considered the gold standard in PEM, do not allow to harness electric power efficiently from the pH gradient between GJ and GM due to the presence of other interfering ions. Therefore, we propose an alternative approach that circumvents this limitation.

## Ion exchange performance of Nafion membranes in aqueous environment

As discussed in the previous section and shown by eqn (1) and (2), maximizing the potential across the membrane is crucial in developing an efficient artificial electric organ.

The electric potential across an ion-selective membrane is typically modeled by the Goldman–Hodgkin–Katz (GHK) equation:[33]

$$V_M = \frac{RT}{F}\ln\left(\frac{\sum_a p_a[a]_{low} + \sum_c p_c[c]_{high}}{\sum_a p_a[a]_{high} + \sum_c p_c[c]_{low}}\right) \quad (5)$$

where the terms [a] and [c] are the molar concentrations of anions and cations present in the low and high salinity compartments of the RED cell, and $p$ are the relative perm-selectivities of the membrane for anions or cations. Perm-selectivity is a specific type of selectivity that quantifies the preference of a membrane for a charged species over a reference species. It is a dimensionless quantity, often expressed as a ratio of permeabilities.[34]

Eqn (5) is valid if only monovalent ions are present. If divalent ions are present in significant amounts, like in most body fluids, the GHK equation takes the extended form presented in Appendix A (eqn (A1)).[35]

We estimated the perm-selectivity values of the Nafion Xion and Nafion® 115 membranes for relevant monovalent ($Cs^+$, $K^+$, $Na^+$, and $Li^+$) and di-valent ($Ca^{2+}$ and $Mg^{2+}$) cations as follows. We used the simple cell presented in Fig. 2A, and we filled one compartment with an HCl solution and the other compartment with solutions of the chloride salts of the cation of interest. We chose the concentrations of these solutions to ensure the same chloride concentration in the two compartments (*e.g.*, 1 M HCl *versus* 0.5 M $MgCl_2$) to minimize the offset potential between the electrodes and the contribution of the chloride ions to $V_M$. Then, we used the measured $V_M$ values to numerically solve the extended GHK equation and obtain the perm-selectivities of the various cations relative to that of the hydronium ion (see Methods for details).

These perm-selectivity values, listed in Table 1 (see Fig. S1†), provide crucial insights into the ion exchange capabilities of Nafion. Both Nafion membranes exhibit a larger selectivity for hydronium ions, as expected, followed by potassium, cesium, sodium, lithium, calcium, and magnesium ions. Both Nafion Xion and Nafion® 115 display significant selectivity for potassium and sodium ions, which explains why the transmembrane potentials generated by GJ and GM were low.

In fact, when used in the extended GHK equation to predict the potential generated by GJ and GM solutions across Nafion membranes, the calculated perm-selectivities yield $V_M$ = 21.2 mV for Nafion® 115 and $V_M$ = 23.4 mV for Nafion Xion, which is in good agreement with the experimental data. Hence, while Nafion membranes are classified as proton exchange membranes, they display poor specificity for protons

**Table 1** Calculated perm-selectivity value

| Membrane | $p_{H_3O^+}$ | Perm-selectivities relative to the hydronium ion | | | | | |
|---|---|---|---|---|---|---|---|
| | | $p_{Cs^+}$ | $p_{Na^+}$ | $p_{K^+}$ | $p_{Li^+}$ | $p_{Ca^{2+}}$ | $p_{Mg^{2+}}$ |
| Nafion XION | 1 | 0.44 ± 0.01 | 0.25 ± 0.01 | 0.58 ± 0.02 | 0.27 ± 0.01 | 0.13 ± 0.01 | 0.13 ± 0.01 |
| Nafion® 115 | 1 | 0.58 ± 0.01 | 0.29 ± 0.02 | 0.74 ± 0.06 | 0.22 ± 0.01 | 0.14 ± 0.01 | 0.13 ± 0.01 |


© 2025 The Author(s). Published by the Royal Society of Chemistry

Open Access Article. Published on 19 2024. Downloaded on 26-06-2025 08:06:16.
This article is licensed under a Creative Commons Attribution-NonCommercial 3.0 Unported Licence.

when employed in aqueous environment, particularly in comparison to potassium and sodium ions (with the term 'proton' we are referring to the hydronium ion $H_3O^+$, as we are always considering aqueous solutions).

To understand the origin of this lack of selectivity, we compared the dry and hydrated structures of the Nafion® 115 and Nafion® Xion using synchrotron small-angle X-ray scattering (SAXS) measurements (Fig. 3A and B, respectively). SAXS is a powerful technique that enables the investigation of the structure of materials from the atomic to the micron scale.[36] While previous literature has explored the structure of Nafion membranes, our focus is on confirming the specific structural characteristics and transport behavior of Nafion® 115 and Xion in hydrated conditions, which have not been comprehensively examined in this context.

The scattering patterns reported in Fig. 3A and B plot the intensity of the scattered light as a function of the scattering vector $q$. The scattering vector depends on the angle at which light is scattered, and its magnitude is inversely proportional to the lengthscale of the features that are being observed (see Methods for details). For example, if structural features of a certain lengthscale $d$ are repeated multiple times within a sample, a peak will be visible in the scattering pattern at approximately $q = 2\pi/d$.

The scattering pattern of dry Nafion® 115 (Fig. 3A) presents a peak at $q \approx 2$ nm$^{-1}$, indicating that a repeating lengthscale of approximately 3 nm is present within the sample. Previous literature[37] attributes this peak to the formation of hydrated ion clusters of ~3 nm size, which form a sort of nanochannel network within the membrane. Upon hydration, the peak shifts towards lower q values and increases in intensity (Fig. 3A), indicating that more clusters have formed while their average size has increased to approximately 3.6 nm. Interestingly, this structural feature is not visible in dry Xion membranes but appears upon hydration (Fig. 3B). The changes in the scattering pattern caused by the hydration of Xion membranes influence a large $q$-range ($0.3 < q < 2.5$), which might be an indication of the interconnected nature of these ion clusters.

The presence of water within the Nafion membranes was confirmed by thermogravimetric analysis (TGA) and contact angle measurements. The TGA profile (Fig. 3C, magenta curve) of a dry Nafion® 115 membrane displays a weight loss at 100 °C of approximately 3%, likely due to the presence of a small amount of entrapped water or moisture absorbed during sample preparation. This observation is consistent with the SAXS data, which also identifies the presence of clusters in the dry state (Fig. 3A). The weight loss becomes significantly larger (approximately 8% at 100 °C) when the membrane has been exposed to water for 48 h, as shown in Fig. 3C (blue curve). Contact angle measurements (Fig. S2†) show no significant difference between dry and hydrated Nafion, corroborating that the larger weight loss of hydrated Nafion is not caused by water adsorbed on the surface of the membrane but by water-rich domains or channels within the membrane.

These SAXS and TGA results explain why Nafion behaves like a CEM, and not as a PEM in aqueous media. Protons – as well as other cations – cross the membrane *via* water-filled channels and not *via* hopping between sulfonate groups, as observed in dry Nafion.[38] To confirm this hypothesis, we recorded *I–V* curves (Fig. 3D and ESI Fig. S3, S4, S5, S6, Tables S2, S3†) and calculated the electrical resistivity of water-swollen Nafion membranes in contact with different electrolyte solutions (see Methods). The resistivity of Nafion membranes to the passage of cations depends linearly (Appendix B) on the apparent hydrodynamic size of the permeating ions (calculated from tabulated diffusion coefficients in water[39,40]). This linearity is consistent with the behavior expected for electrophoretic diffusion through aqueous channels, where the electrophoretic mobility scales linearly with the inverse of the hydrodynamic size of the ions.[41]

We note that the resistivity value measured at 1 M HCl follows the same linear trend of the other cations because we calculated the apparent hydrodynamic size of hydrated protons from their experimental diffusion coefficient, which incorporates contributions from both diffusion and hopping (Grotthuss mechanism).[39] As shown in Fig. 3E and F, we demonstrate this linear relationship for both Nafion® 115 and Xion in the presence of various monovalent cations, including the hydronium ion, corroborating that proton/ion transport in wet Nafion occurs *via* water-filled channels.

### Towards an implantable artificial electric organ

Despite the significant proton gradient between GJ and GM, the electrical potential generated by these solutions across Nafion membranes is small. To circumvent this problem, we evaluated the use of ionic gradients between gastric juices and potable water, as water is regularly ingested to sustain life. Using the same experimental setup described in Fig. 2A and the Methods section, we measured the $V_{OC}$ across the Nafion membranes when a solution mimicking potable water ($[Na^+] = 2 \times 10^{-3}$ M; $[K^+] = 5 \times 10^{-5}$ M; $[Cl^-] = 5.05 \times 10^{-3}$ M; $[HCO_3^-] = 2 \times 10^{-3}$ M; $[H_3O^+] = 2.5 \times 10^{-8}$ M, pH = 7.6; $[Ca^{2+}] = 2 \times 10^{-3}$ M; $[Mg^{2+}] = 5 \times 10^{-4}$ M; $[OH^-] = 4.0 \times 10^{-7}$ M; fixed residue = 0.495 g L$^{-1}$) was used as an ion-poor solution against the GJ mimic. We obtained values of $V_{OC} = 200 \pm 2$ mV for Nafion® 115 and $V_{OC} = 170 \pm 1$ mV for Nafion Xion (see Fig. S7†). Considering the offset potential of the electrodes ($V_{EL} = 89$ mV calculated using eqn (3)), we estimated the values of $V_M = 111 \pm 2$ mV and a maximum power density of $PD_M = 20 \pm 3$ mW m$^{-2}$ for Nafion® 115, and $V_M = 81 \pm 1$ mV and $PD_M = 13 \pm 1$ mW m$^{-2}$ for Nafion Xion. We used the extended GHK equation (Appendix A) to estimate the theoretical values of the expected transmembrane potentials for the system that includes divalent ions too. The calculated values are in good agreement with the experimental results ($V_M = 119$ mV for Nafion® 115 and $V_M = 98$ mV for Nafion Xion).

Overall, the $PD_M$ values obtained with the potable water and gastric juices mimics significantly surpass those obtained with gastric mucous (see Fig. 2D). We also tested a commercial drinking water (Tavina S.p.A.; Rotatoria Cav. Tonoli Amos, 2; 25087 Salò (BS), Italy), and obtained comparable power densities (considering the offset potential of the electrodes

Open Access Article. Published on 19 2024. Downloaded on 26-06-2025 08:06:16.
This article is licensed under a Creative Commons Attribution-NonCommercial 3.0 Unported Licence.

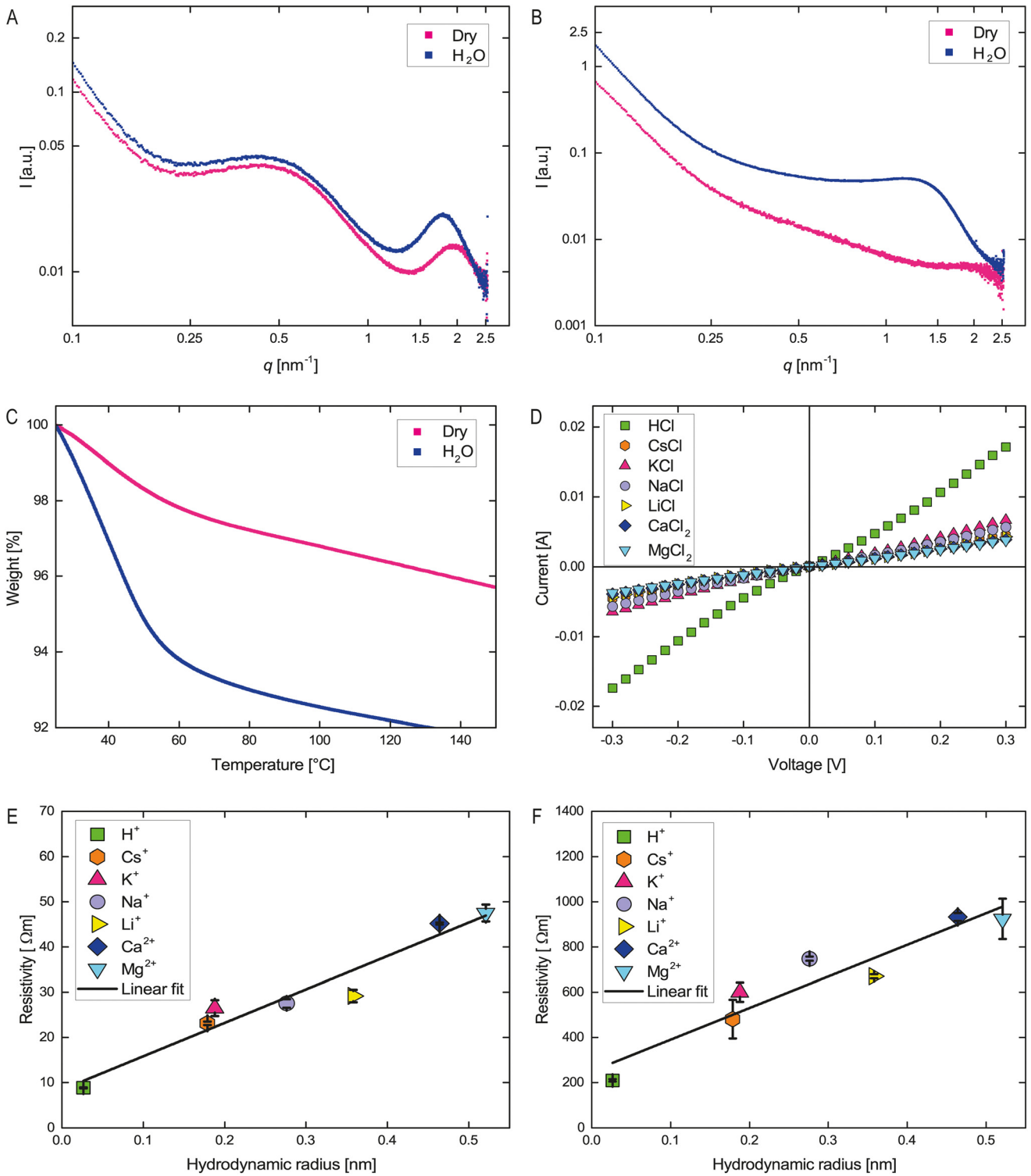


**Fig. 3** (A and B) Small-angle X-ray scattering (SAXS) characterization of (A) Nafion® 115 and (B) Nafion Xion. (C) Thermogravimetric analysis of two samples of Nafion® 115. Both samples were exposed to a conditioning cycle in distilled water for two hours and a drying cycle in the oven at 60 °C for two hours. Subsequently, one sample was rehydrated in deionized water ($H_2O$) and the other sample was dried in a desiccator under vacuum (Dry) for two days. (D) Transmembrane current as a function of the applied potential (*I*–*V* curves) for Nafion® 115 membranes exposed to various salt solutions. The concentration of monovalent salts was 1 M, while the concentration of divalent salts was 0.5 M. (E and F) Resistivity values calculated from the *I*–*V* curves in D as a function to the apparent hydrodynamic radius for (E) Nafion® 115 and (F) Nafion Xion. The apparent hydrodynamic radii were calculated from the diffusion coefficients of the various ions in water.[39,40] In both graphs, the solid lines are linear fitting.


© 2025 The Author(s). Published by the Royal Society of Chemistry

Open Access Article. Published on 19 2024. Downloaded on 26-06-2025 08:06:16.
This article is licensed under a Creative Commons Attribution-NonCommercial 3.0 Unported Licence.

$V_{EL}$ = 147 mV calculated using eqn (3), $PD_M$ = 35 ± 6 mW $m^{-2}$ and $V_M$ = 154 ± 2 mV for Nafion® 115, and $PD_M$ = 15 ± 1 mW $m^{-2}$ and $V_M$ = 101 ± 2 mV for Nafion Xion) (see Fig. S7†). Encouraged by these results, we assembled a RED cell stack under flow using Nafion® 115 as the CEM, commercial Fumasep® FAB-PK-130 μm as the AEM, the GJ mimic as ion-rich solution, and the potable water mimic as low-salt solution (Fig. 4D). We assembled the device as reported in Fig. 4E (see Methods for details). We tested RED stacks comprising 1, 2, and 3 cells. Fig. 4A–C and Fig. S8A–C† plot the obtained values of $V_{OC}$, $r$ and $PD_{max}$ as a function of the number of stacked cells under flow.

Since $V_{OC}$ is proportional to the number of cells ($n_{cell}$) and since the electrode potential offset is negligible in this setup, a linear fitting of the $PD_{max}$ yields the maximum power density per cell of the device ($PD_{cell}$):

$$PD_{max} = \frac{V_{OC}^2}{4rA} = n_{cell}\frac{V_{cell}^2}{4rA} = n_{cell}PD_{cell} \quad (6)$$

We obtained values of $V_{cell}$ = 134 mV and $PD_{cell}$ = 188 mW $m^{-2}$ when operating under continuous flow conditions with water as the ion-poor solution and gastric juices as the ion-rich solution. In theory, the power and voltage generated by stacking 23 cells in series should be sufficient to aliment a pacemaker, which typically requires approximately 3 V and 20 μW to function.

The power density values obtained with this device are approximately 10 times smaller than high-performance, RED-based hydrogel power units ($PD_{cell}$ = 1.8 W $m^{-2}$).[7] Hydrogel batteries, however, are prepared using high salt concentrations (6 M), significantly higher than typical physiologic ion concentrations, which are not available under physiologic conditions inside living organisms. Conventional reverse electrodialysis using river and sea water typically yields power densities around 4 W $m^{-2}$.[42] We expect that the system presented here can approach this performance by using membranes with improved proton selectivity and designing thinner compartments to reduce internal resistance. Compared to RED-based devices that convert physiologic byproducts (*e.g.* exhaled $CO_2$ from breath, $PD_{cell}$ = 30 mW $m^{-2}$),[15] the device presented here displays significantly superior performance. Regarding absolute power output, the device presented here delivers approximately 19 μW per cell. Combining multiple cells, we can match or exceed the power output of several implantable energy harvesters, such as piezoelectric systems that capture kinetic energy and can achieve peak voltages around 8 V, with power densities of up to 12 mW $m^{-2}$. Biofuel cells typically operate at 190 mV and 96 mW $m^{-2}$. Thermal energy harvesters, which rely on temperature differences of approximately 40° C (a challenging condition to achieve within the human body), can reach power densities as high as 19 W $m^{-2}$. On the other hand, radio frequency energy harvesting systems outperform the device presented here by delivering power densities on the order of 280 mW $m^{-2}$. Implantable photovoltaic cells can generate up to 4 W $m^{-2}$, but due to the implantation losses, they have low efficiencies (about 1%), and their effective power densities are typically around 40 mW $m^{-2}$.[2]

The technology presented in this work holds significant promise for powering low-energy prosthetic devices like pacemakers. In the future, using fluorine-free membranes with superior proton selectivity and further optimization of the device geometry may afford significantly larger power outputs, potentially making electric power generation from physiologic ion gradients an attractive strategy to power active prosthetic devices.

# Experimental

### Materials and equipment

We purchased all chemicals from Sigma-Aldrich (Merck-KGaA). We obtained Xion PEM-Nafion-1100 (5 μm thick) from FFI-Ionix, and we acquired the Nafion® 115 perfluorinated membrane (thickness 0.005 in −127 μm thick) from Sigma-Aldrich (Merck-KGaA). We purchased the anion exchange membrane Fumasep® FAB-PK-130 PEEK-reinforced (130 μm thick) from Fumatech – functional membranes for fuel cells (BWT group). We 3D printed the RED compartments and the compartments for all other measurements with a Form 3 3D printer (Formlabs Inc.) using Clear Resin V4 from the same producer. We purchased silver wires (0.5 mm diameter) and silver plates (1 mm thick) from Sigma-Aldrich (Merck-KGaA) and Thermo Fisher (Kandel) GmbH, respectively. We purified the water to 18.2 MΩ cm with a PURELAB Flex II purifier (ELGA LabWater, Veolia).

### Solutions

We prepared the two mimicking gastric solutions (gastric juices and gastric mucous) according to the literature,[16,17] excluding the components that increase their viscosity; while water was prepared based on the fixed residue of commercially available water, Tavina. The compositions of the solutions are the following:

- gastric mucus ($[Na^+]$ = 0.124 M; $[K^+]$ = 0.005 M; $[Cl^-]$ = 0.127 M; $[HCO_3^-]$ = 0.002 M; $[H_3O^+] = 2.2 \times 10^{-8}$ M; $[OH^-] = 4.5 \times 10^{-7}$ M; pH = 7.6).
- gastric juices ($[Na^+]$ = 0.149 M; $[H_3O^+]$ = 0.047 M; $[Cl^-]$ = 0.196 M; $[OH^-] = 2.1 \times 10^{-13}$ M; pH = 1.3).
- Tavina water – reported on the bottle ($[Na^+] = 8.3 \times 10^{-4}$ M; $[K^+] = 5.1 \times 10^{-5}$ M; $[NO^{3-}] = 4.8 \times 10^{-5}$ M; $[HCO_3^-] = 6.1 \times 10^{-3}$ M; $[H^+] = 2.5 \times 10^{-8}$ M; $[Ca^{2+}] = 1.8 \times 10^{-3}$ M; $[Mg^{2+}] = 1.1 \times 10^{-3}$ M); fixed residue = 0.363 g $L^{-1}$ at 180 °C; pH = 7.6. From the difference between the reported concentrations of cations and anions, we estimated $[Cl^-] = 5.3 \times 10^{-4}$ M.
- water ($[Na^+] = 2 \times 10^{-3}$ M; $[K^+] = 5 \times 10^{-5}$ M; $[Cl^-] = 5.05 \times 10^{-3}$ M; $[HCO_3^-] = 2 \times 10^{-3}$ M; $[H_3O^+] = 2.5 \times 10^{-8}$ M; $[Ca^{2+}] = 2 \times 10^{-3}$ M; $[Mg^{2+}] = 5 \times 10^{-4}$ M; $[OH^-] = 4.0 \times 10^{-7}$ M); fixed residue = 0.495 g $L^{-1}$; pH = 7.6.

### Electrodes

We selected the redox reaction of Ag/AgCl to convert ionic currents to electric currents. The standard electrode potential of

Open Access Article. Published on 19 2024. Downloaded on 26-06-2025 08:06:16.
This article is licensed under a Creative Commons Attribution-NonCommercial 3.0 Unported Licence.

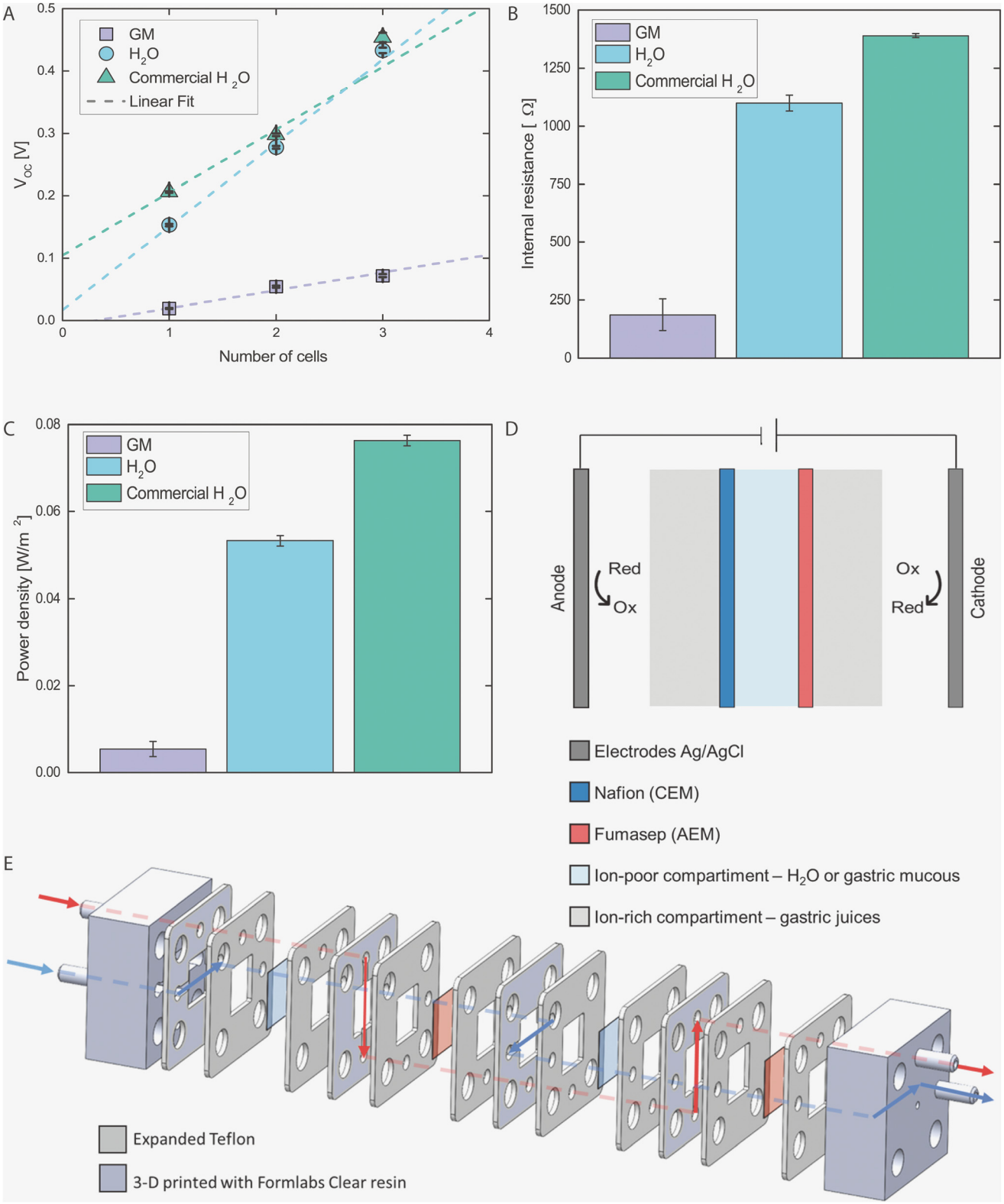


**Fig. 4** (A) Comparison of the open circuit potentials obtained with Nafion® 115 in a RED cell with the setup reported in (E) as a function of the number of cells stacked in series. (B) Comparison of the internal resistances of a single cell using different ion lean solutions. (C) Comparison of the power densities related to a single cell calculated from the internal resistances and potentials following eqn (6). (D) Schematic representation of the repetitive unit cell used to assemble a RED system. (E) Optimized device with multiple flow cells stacked in series. The arrows in red and blue refer to the path that ion-rich and ion-lean solutions follow inside the cell.


© 2025 The Author(s). Published by the Royal Society of Chemistry

Open Access Article. Published on 19 2024. Downloaded on 26-06-2025 08:06:16.
This article is licensed under a Creative Commons Attribution-NonCommercial 3.0 Unported Licence.

Ag/AgCl is $E_0$ = 0.230 V *versus* the standard hydrogen electrode (SHE). To prepare the two electrodes, we used a solution of KCl 1 M, a platinum wire, two silver wires or two silver plates (as specified in the section electrical characterization), and a Keithley 2400 Source Meter (Keithley Instruments). We electrically connected the two silver wires or the two silver plates to reduce the offset potential between them, immersed them in the KCl solution, and connected them to the cathode of the instrument. Subsequently, we applied a potential of 3 V using a platinum counter-electrode. A layer of AgCl formed on the surface of the silver materials.

### 3D printing

We modeled all the cells used for the electrical characterization and all terminal compartments for electrodes using the software SolidWorks (Dassault Systemes). We 3D printed the 3D models (see ESI Fig. S9, S10, and S11†) with a Form 3 (Formlabs Inc.) printer, which uses a stereolithographic technique, in an acrylic transparent resin known commercially as Formlabs Clear. After manufacturing, we washed the 3D printed parts in isopropanol for up to two hours to remove excess uncured resin and then post-cured *via* the irradiation with UV light (365 nm wavelength, 14 W $cm^{-2}$ power) using an LEDcube100 and PowerDrive chamber and lamp driver (Hoenle).

### Electrical characterization

In all measurements, we used 3D printed cells with two chambers (see Fig. S9 and S10†) and assembled them with the Nafion membrane in the middle to divide the two compartments. We ensured hermetic sealing with two expanded Teflon gaskets. We filled the chambers with either 1 mL (compartments in Fig. S9†) or 5 mL of solution (compartments in Fig. S10†) and used Ag/AgCl plate electrodes. Before each *I–V* curve and perm-selectivity measurement, we performed an ion-conditioning process on the membranes to reduce the contribution of residual protons. We first equilibrated each membrane in MilliQ water for at least 2 hours. After equilibration, we dried the membranes at 60 °C for 30 minutes, after which we conditioned the Nafion membranes in a solution of the target salt (1 M for monovalent and 0.5 M solution for divalent cations) for 30 minutes to ensure the conductive properties were dominated by the cation species of interest rather than protons. After this time, the membrane is gently wiped with absorbent paper (Kimtech) and mounted in the measurement cell.

We recorded the *I–V* plots of the Nafion membranes using a Keithley 2400 Source Meter. We prepared Ag/AgCl plate electrodes just before the measurements. We used two pieces (2 × 2 $cm^2$) of expanded Teflon (1 mm thick) with holes (0.5 cm Ø) in the centers to form gaskets. We cut a (1.2 × 1.2 $cm^2$) piece of Nafion and sandwiched it between the two Teflon parts. We then assembled the 3D printed cell (see Fig. S10†) with the gaskets and the Nafion membrane separating the two chambers.

We recorded *I–V* relationships for both symmetric and asymmetric cases. Symmetric meaning that two compartments of the cell were filled with the same salt solution (*i.e.*, HCl *vs.* HCl; CsCl *vs.* CsCl; KCl *vs.* KCl; NaCl *vs.* NaCl; LiCl *vs.* LiCl; $CaCl_2$ *vs.* $CaCl_2$; $MgCl_2$ *vs.* $MgCl_2$; all the monovalent salt solutions were 1 M in concentration, while the divalent salt solutions were 0.5 M in concentration). Asymmetric meaning that the two chambers were filled with two different salt solutions (*i.e.*, HCl *vs.* KCl; HCl *vs.* NaCl; HCl *vs.* $CaCl_2$; HCl *vs.* $MgCl_2$; all the monovalent salt solutions were 1 M in concentration, while the divalent salt solutions were 0.5 M in concentration). We tested both cases for Nafion® 115 and Nafion Xion.

For the asymmetric *I–V* curves, we filled the compartment of the chamber with the anode using the salt solution of interest and inserted the electrode of the Mettler Toledo SevenCompact Duo pH meter into the solution. We monitored the pH during the measurement to ensure no significant changes occurred over time. We applied voltages ranging from −300 to 300 mV in steps of 20 mV (starting from 0 and then alternating the polarity for each value of voltage: −20, 20, −40, 40, ..., −300, 300). Instead, for the symmetric *I–V* curves, we filled the two compartments of the cell with the same solution of interest.

We estimated the power density by measuring the open circuit voltage ($V_{OC}$) and the voltage across a resistor ($V_{Load}$) using an electrical circuit (see Fig. S12†) with a switcher that allowed to measure the $V_{OC}$ and then the voltage through a 4700 Ω resistor ($r_{Load}$). The setup was the same as described in the section related to *I–V* plots, except for the cell (see Fig. S9†) and the gaskets, which had a hole (1 × 1 $cm^2$) in the center. With these measured values, we calculated the internal resistance ($r$ [Ω]) of the cell using the following equation:

$$r = r_{Load}\left(-1 + \frac{V_{OC}}{V_{Load}}\right), \quad (7)$$

and estimated the power density of the device according to eqn (6).

### Estimating relative perm-selectivity

We estimated the perm-selectivity values of the Nafion Xion and Nafion® 115 membranes for relevant monovalent ($Cs^+$, $K^+$, $Na^+$ and $Li^+$) and di-valent ($Ca^{2+}$ and $Mg^{2+}$) cations as follows: we used the simple cell presented in Fig. 2A (and see Fig. S10†) and we filled one compartment with an HCl solution and the other compartment with solutions of the chloride salts of the target cations. We chose the concentrations of these solutions to ensure the same chloride concentration in the two compartments (*e.g.* 1 M HCl *versus* 0.5 M $MgCl_2$), thereby minimizing the offset potential between the electrodes and the contribution of the chloride ions to $V_M$. Then we used the measured $V_M$ values to solve the extended GHK equation numerically (eqn (8)–(12)) using Python, and a custom-made script based on the LMFIT package (**https://lmfit.github.io/lmfit-py/**). The input parameters for the script are the concentrations of the various ions and the pH of the two compartments. We verified that the perm-selectivities were independent of the salt concentration (see Fig. S13†).

Open Access Article. Published on 19 2024. Downloaded on 26-06-2025 08:06:16.
This article is licensed under a Creative Commons Attribution-NonCommercial 3.0 Unported Licence.

### RED flow system assembly

Fig. 4E (and Fig. S11† for details) shows the flow system. We 3D printed the compartments and the terminal compartments that host the electrodes with the same 3D printer as above and cut the gaskets from expanded Teflon. Each terminal compartment has two cylindrical prominences to connect with the flow tubing, allowing us to pump solutions in and out of the system. Additionally, we added an extra hole to the terminal compartments to connect the electrodes through a silver wire to the source meter. Leakages were prevented by sealing the electrode hole with a hot-melt adhesive. We alternated the AEM (Fumasep® FAB-PK-130 PEEK-reinforced, 130 μm thick) and the CEM (Nafion® 115), sandwiched in between expanded Teflon gaskets to avoid leakages. We designed the electrodes using a silver wire and modeled them with a square spiral shape to fit inside the cubic blind hole of the terminal compartments. After stacking the components in the correct order (see Fig. 4E and Fig. S11†), we closed the system with screws and bolts, applying torque until no leakages were observed. We used a Gilson MP3 peristaltic pump with a 2-channel pumping head to generate a flow of 1.5 mL $min^{-1}$ for the two solutions (gastric juices *vs.* gastric mucous or drinkable water mimics). We used Gilson's PVC tubing (1.2 mm internal diameter) to inject the solutions into the RED cell. Finally, we connected the source meter to the electrodes and used it to record the open circuit voltage and the voltage across an external 4700 Ω resistor. We estimated the power density as described in the previous section.

### Contact angle measurements

We performed contact angle measurements using the sessile drop method with a Dataphysics OCA-15 Pro contact angle analyzer. We dispensed 2 μL of distilled water in the form of a drop on the sample. We then processed the digital image with an image analysis system, which calculated both the left and right contact angles based on the shape of the drop. We derived the final value from the average of the angles measured on both sides of the droplet. We tested multiple stripes (0.5 × 3 $cm^2$) of Nafion® 115 and Nafion Xion. Before testing, we kept all samples in distilled water for two hours, heated them in an oven at 60 °C for two hours, and then differentiated them as follows:

$H_2O$: we placed the samples in MilliQ water, removed them just before measurement, and dried the residual water with a paper towel.

Dry: we dried the samples in a desiccator under vacuum and then tested them.

### Thermogravimetric analysis

We conducted thermogravimetric analyses (TGA) under a nitrogen atmosphere in a temperature range of 25 to 150 °C, with a heating rate of 10 °C $min^{-1}$, using a Mettler-Toledo STAR thermogravimetric analyzer. We prepared the samples using around 10 mg of Nafion® 115, which was kept in distilled water for at least two hours and then heated in an oven at 60 °C for two hours. Afterward, we differentiated the samples by placing one in distilled water and the other one in a desiccator under vacuum, both for two days. Finally, we performed the measurements.

### SAXS

We performed SAXS measurements at the ID02 Beamline in Grenoble.[43] We calibrated the sample-to-detector distance using Ag-behenate crystals and the acquired 2D data were azimuthally averaged using a software provided by the beamline. We prepared samples of the two Nafion membranes by keeping them in distilled water for at least two hours, followed by heating them in an oven at 60 °C for two hours. We then differentiated the samples by placing one in distilled water and the other in a desiccator under vacuum, both for two days.

### Statistical analysis

We freshly prepared the solutions for each measurement. We conditioned the membranes in distilled water for at least two hours before use. We repeated all measurements at least three times, and we presented the data as the mean ± standard deviation (SD), except for SAXS and TGA measurements.

## Conclusions

This work evaluates the use of Nafion membranes in the assembly of a bioinspired artificial electric organ capable of generating electric power from the proton gradient present between gastric juices and gastric mucous in the stomach. First, we investigated the mechanism of ion transport across Nafion membranes in aqueous environments. By comparing the dry and hydrated structures of the membranes using various techniques (including SAXS, contact angle measurements, and TGA), we observed significant structural changes upon hydration that elucidated why Nafion behaves as a cation-selective membrane in aqueous media. Hydronium ions and other cations can cross the membrane *via* water-filled channels. This transport mechanism is very different from the proton hopping between sulfonate groups observed in dry Nafion. Hydrated Nafion membranes display a linear relationship between electrical resistivity and the apparent hydrodynamic size of the dissolved ions, confirming that ion transport occurs *via* electrophoresis and diffusion (and *via* Grotthuss mechanism for protons) through water-filled channels. Subsequently, we calculated the perm-selectivity values of Nafion membranes towards biologically relevant cations, such as $Na^+$ and $K^+$, and we used these values to optimize an artificial electric organ that can deliver enough power to sustain small biomedical devices when supplied with gastric juices and drinkable water mimics ($V_{cell}$ = 134 mV and $PD_{cell}$ = 188 mW $m^{-2}$). The application of this technology to power larger devices such as active prosthetics will likely require the use of an auxiliary battery that is continuously recharged by the electric organ (for instance, during sleep hours) and can supply larger amounts of power on demand.


© 2025 The Author(s). Published by the Royal Society of Chemistry

Open Access Article. Published on 19 2024. Downloaded on 26-06-2025 08:06:16.
This article is licensed under a Creative Commons Attribution-NonCommercial 3.0 Unported Licence.

While the use of fluorinated polymers is being questioned due to environmental and health-related issues, the results reported in this work demonstrate the potential of reverse electrodialysis as a strategy to harvest metabolic energy. Moreover, this work suggests one possible strategy towards the realization of implantable power units that use biocompatible and sustainable charge-selective membranes to generate electric power from physiological ion gradients, with the ultimate goal of providing a continuous energy supply to implanted devices and prosthetics.

## Author contributions

Carolina Pierucci: data curation, formal analysis, investigation, methodology, validation, writing – original draft, writing – review & editing. Lorenzo Paleari: software. James Baker: formal analysis, investigation, methodology. Christian C. M. Sproncken: writing – review & editing. Matilde Folkesson: writing – review & editing. Justus Paul Wesseler: writing – review & editing. Andela Vracar: investigation, writing – review & editing. Andrea Dodero: investigation, writing – review & editing. Francesca Nanni: supervision, writing – review & editing. José Augusto Berrocal: supervision, writing – review & editing. Michael Mayer: supervision, writing – review & editing. Alessandro Ianiro: data curation, formal analysis, methodology, project administration, software, supervision, validation, writing – original draft, writing – review & editing.

## Data availability

The data that support the findings of this study are openly available in Zenodo repository at **https://zenodo.org/uploads/13833499**.

## Conflicts of interest

There are no conflicts to declare.

## Appendix A

The GHK equation (eqn (5) main text) is valid when only monovalent ions are present in the system. This expression needs to be adjusted when divalent ions are present:[35]

$$V_M = \frac{RT}{F}\ln\left(\frac{[S_1 - T_1] + \sqrt{[S_1 + T_1]^2 + 16[T_1S_2 + T_2S_1 + 4T_2S_2]}}{2[T_1 + 4T_2]}\right) \quad (8)$$

where $S1$, $T1$, $S2$ and $T2$ are given by the following equations:

$$S_1 = p^{Naf}_{Na^+}[Na^+]_{low} + p^{Naf}_{K^+}[K^+]_{low}; \quad (9)$$

$$T_1 = p^{Naf}_{Na^+}[Na^+]_{high} + p^{Naf}_{H^+}[H^+]_{high}; \quad (10)$$

$$S_2 = p^{Naf}_{Ca^{2+}}[Ca^{2+}]_{low} + p^{Naf}_{Mg^{2+}}[Mg^{2+}]_{low}; \quad (11)$$

$$T_2 = p^{Naf}_{Ca^{2+}}[Ca^{2+}]_{high} + p^{Naf}_{Mg^{2+}}[Mg^{2+}]_{high}; \quad (12)$$

where the subscript 'Naf' indicates the Nafion membrane.

## Appendix B

In aqueous solutions, resistivity ($\rho$) is directly proportional to the hydrodynamic radius ($R_H$) of the ions. In order to verify this hypothesis, this relation can be derived by considering the definition of electrophoretic mobility ($\mu_e$), that is a measure of the velocity of a charged particle under the influence of an electric field. It describes how quickly the particle moves in a fluid medium when subjected to an electric field:

$$\mu_e = \frac{v}{E} \quad (13)$$

where $\nu$ is the drift velocity in m $s^{-1}$ of a dispersed particle and it is given by the following expression:

$$v = \frac{zeE}{f} \quad (14)$$

In which $z$ is the valence of the ion, $e$ is the elementary charge, $E$ is the electric field strength in V $m^{-1}$ and $f$ is the frictional coefficient in kg $s^{-1}$, a parameter that quantifies the drag resistance experienced by a particle that moves through a medium. The frictional coefficient of a sphere with a hydrodynamic radius $R_H$ in a fluid with dynamic viscosity $\eta$ is:

$$f = 6\pi\eta R_H \quad (15)$$

Substituting eqn (14) and (15) in eqn (1), the electrophoretic mobility becomes:

$$\mu_e = \frac{ze}{6\pi\eta R_H} \quad (16)$$

The electrical conductivity ($\sigma$) in S $m^{-1}$, as a measure of the ability of a material to conduct an electric current, can be expressed as:

$$\sigma = F\sum_i c_i j_i \mu_{ei}, \quad (17)$$

where $c_i$ is the molar concentration of ion i, $j_i$ is the stoichiometric coefficient of the dissociation reaction of ion i, $F$ is the Faraday constant. Using eqn (16), we can rewrite eqn (17) as follows:

$$\sigma = \frac{Fe}{6\pi\eta}\sum_i \frac{c_i j_i z_i}{R_{Hi}} \quad (18)$$

Using eqn (18), the resistivity ($\rho$) of a charge-selective membrane in the presence of a single electrolyte, can be approximated by:

$$\rho = \frac{1}{\sigma} \approx \frac{6\pi\eta R_H}{Fcjze} \quad (19)$$

Open Access Article. Published on 19 2024. Downloaded on 26-06-2025 08:06:16.
This article is licensed under a Creative Commons Attribution-NonCommercial 3.0 Unported Licence.

If we define an equivalent charge concentration as $k = cz$, we can write eqn (19) as:

$$\rho \approx \frac{6\pi\eta R_H}{Fkej}. \quad (20)$$

Hence, assuming that the stoichiometric coefficient $j_i$ of the dissociation reaction of ions, i and $k$ are constant, the resistivity of the membrane should scale linearly with the hydrodynamic radius of the selected ion:

$$\rho \sim R_H. \quad (21)$$

## Acknowledgements

This work was financially supported by the Pathfinder Open project INTEGRATE (grant number 101046333), co-financed by the European Innovation Council (EIC) and the Swiss State Secretariat for Education, Research and Innovation (SERI) and by the Adolphe Merkle Foundation. The authors acknowledge the European Synchrotron Radiation Facility (ESRF), Grenoble, France, for granting beamtime on beamline ID02 through the proposal SC-5454 and would like to thank Dr Theyencheri Narayanan and Dr Gouranga Manna for their assistance during the scattering experiments. The authors thank Dr Pau Bachs Molet for the useful discussion on the structure of the membranes.

## References

1 Standards for prosthetics and orthotics, World Health Organization, 2017.
2 J. Zhao, R. Ghannam, K. O. Htet, Y. Liu, M. Law, V. A. L. Roy, B. Michel, M. A. Imran and H. Heidari, *Adv. Healthc. Mater.*, 2020, **9**, 2000779.
3 A. Cadei, A. Dionisi, E. Sardini and M. Serpelloni, *Meas. Sci. Technol.*, 2014, **25**, 012003.
4 X. Huang, L. Wang, H. Wang, B. Zhang, X. Wang, R. Y. Z. Stening, X. Sheng and L. Yin, *Small*, 2020, **16**, 1902827.
5 A. L. Gotter, M. A. Kaetzel and J. R. Dedman, *Comp. Biochem. Physiol., Part A:Mol. Integr. Physiol.*, 1998, **119**, 225–241.
6 T. B. H. Schroeder, A. Guha, A. Lamoureux, G. VanRenterghem, D. Sept, M. Shtein, J. Yang and M. Mayer, *Nature*, 2017, **552**, 214–218.
7 A. Guha, T. J. Kalkus, T. B. H. Schroeder, O. G. Willis, C. Rader, A. Ianiro and M. Mayer, *Adv. Mater.*, 2021, **33**, 2101757.
8 J. N. Weinstein and F. B. Leitz, *Science*, 1976, **191**, 557–559.
9 R. E. Lacey, *Ocean Eng.*, 1980, **7**, 1–47.
10 P. Długołcki, A. Gambier, K. Nijmeijer and M. Wessling, *Environ. Sci. Technol.*, 2009, **43**, 6888–6894.
11 J. Ran, L. Wu, Y. He, Z. Yang, Y. Wang, C. Jiang, L. Ge, E. Bakangura and T. Xu, *J. Membr. Sci.*, 2017, **522**, 267–291.
12 N. H. Othman, N. Kabay and E. Guler, *Rev. Chem. Eng.*, 2022, **38**, 921–958.
13 H. B. Park, J. Kamcev, L. M. Robeson, M. Elimelech and B. D. Freeman, *Science*, 2017, **356**, 1138–1148.
14 J. Xu and D. A. Lavan, *Nat. Nanotechnol.*, 2008, **3**, 666–670.
15 T. J. Kalkus, A. Guha, P. B. V. Scholten, D. Nagornii, A. Coskun, A. Ianiro and M. Mayer, *Adv. Sci.*, 2021, **8**, 2100995.
16 C. Hoebler, G. Lecannu, C. Belleville, M.-F. Devaux, Y. Popineau and J.-L. Barry, *Int. J. Food Sci. Nutr.*, 2002, **53**, 389–402.
17 B. Yao, D. L. Hogan, K. Bukhave, M. A. Koss and J. I. Isenberg, *Gastroenterology*, 1993, **104**, 732–740.
18 S. J. Sondheimer, N. J. Bunce and C. A. Fyfe, *J. Macromol. Sci., Part C: Polym. Rev.*, 1986, **26**, 353–413.
19 P. Choi, N. H. Jalani and R. Datta, *J. Electrochem. Soc.*, 2005, **152**, E123.
20 A. Paspureddi, Z. Zhang, V. Ganesan, M. M. Sharma and L. E. Katz, *J. Chem. Phys.*, 2023, **158**, 214904–214901.
21 S. J. Paddison and R. Paul, *Phys. Chem. Chem. Phys.*, 2002, **4**, 1158–1163.
22 K. Schmidt-Rohr and Q. Chen, *Nat. Mater.*, 2008, **7**, 75–83.
23 S. R. Samms, S. Wasmus and R. F. SavineII, *J. Electrochem. Soc.*, 1996, **143**, 1498.
24 L. Maldonado, J.-C. Perrin, J. Dillet and O. Lottin, *J. Membr. Sci.*, 2012, **389**, 43–56.
25 S. G. A. Flimban, S. H. A. Hassan, Md. M. Rahman and S.-E. Oh, *Int. J. Hydrogen Energy*, 2020, **45**, 13643–13651.
26 S. Jacobs and D. S. Kosson, *Assessment of Fluoropolymer Production and Use With Analysis of Alternative Replacement Materials*, Savannah River Site, Aiken,USA, 2024.
27 Y. Xiang, M. Yang, Z. Guo and Z. Cui, *J. Membr. Sci.*, 2009, **337**, 318–323.
28 Hydrogen Europe Position Paper on PFAS, 2023.
29 H. Kahraman and Y. Akın, *Energy Convers. Manage.*, 2024, **304**, 118244.
30 M. B. Karimi, F. Mohammadi and K. Hooshyari, *Int. J. Hydrogen Energy*, 2019, **44**, 28919–28938.
31 S. N. Makarov, R. Ludwig and S. J. Bitar, *Practical Electrical Engineering*, Springer, 2016.
32 W. Nernst, *Theoretical Chemistry from the Standpoint of Avogardro's Rule & Thermodynamics*, Macmillan and Company, 1895.
33 A. L. Hodgkin and B. Katz, *J. Physiol.*, 1949, **108**, 37–77.
34 T. Sata, R. Yamane and Y. Mizutani, *J. Polym. Sci., Polym. Chem. Ed.*, 1979, **17**, 2071–2085.
35 W. F. Pickard, *Math. Biosci.*, 1976, **30**, 11.
36 T. Narayanan, M. Sztucki, P. Van Vaerenbergh, J. Léonardon, J. Gorini, L. Claustre, F. Sever, J. Morse and P. Boesecke, *J. Appl. Crystallogr.*, 2018, **51**, 1511–1524.
37 J. A. Elliott, S. Hanna, A. M. S. Elliott and G. E. Cooley, *Macromolecules*, 2000, **33**, 4161–4171.
38 A. Kusoglu and A. Z. Weber, *Chem. Rev.*, 2017, **117**, 987–1104.


© 2025 The Author(s). Published by the Royal Society of Chemistry

Open Access Article. Published on 19 2024. Downloaded on 26-06-2025 08:06:16.
This article is licensed under a Creative Commons Attribution-NonCommercial 3.0 Unported Licence.

39 N. Amdursky, Y. Lin, N. Aho and G. Groenhof, *Proc. Natl. Acad. Sci. U. S. A.*, 2019, **116**, 2443–2451.
40 P. C. F. Pau, J. Berg and W. G. Mcmillan, *J. Phys. Chem.*, 1990, **94**, 2671–2679.
41 R. L. Cunico, K. M. Gooding and T. Wehr, *Basic HPLC and CE of Biomolecules*, Bay Bioanalytical Laboratory, Richmond (CA), 1998.
42 T. F. Gül, M. Akalın, E. N. Dönmezler, A. Bolat, A. Cihanoğlu, E. Güler and N. Kabay, *Front. Membr. Sci. Technol.*, 2024, **3**, 1414721.
43 T. Narayanan, M. Sztucki, T. Zinn, J. Kieffer, A. Homs-Puron, J. Gorini, P. Van Vaerenbergh and P. Boesecke, *J. Appl. Crystallogr.*, 2022, **55**, 98–111.